Computational Materials Science 111 (2016) 157–162

Contents lists available at ScienceDirect

Computational Materials Science

journal homepage: www.elsevier.com/locate/commatsci

Editor's Choice

Critical stress for the bcc–hcp martensite nucleation in Ti–6.25at.%Ta and Ti–6.25at.%Nb alloys

A. Ojha, H. Sehitoglu *

Department of Mechanical Science and Engineering, University of Illinois at Urbana-Champaign, 1206 W. Green St., Urbana, IL 61801, USA

ARTICLE INFO

Article history:
Received 18 April 2015
Received in revised form 6 August 2015
Accepted 25 August 2015

Keywords:
Ti–Ta
Ti–Nb
Martensite
bcc
hcp
Phase transformation
Peierls–Nabarro

ABSTRACT

Martensitic transformation is an important deformation mechanism in titanium alloys. Using density functional theory calculations, we establish the lattice constants and the associated energetics of the bcc–hcp transformation in Ti–6.25at.%Ta and Ti–6.25at.%Nb alloys. We present a bcc–hcp nucleation model based on the Peierls Nabarro formalism, incorporating the elastic strain energy of the dislocations participating in the transformation process, and subsequently obtain the theoretical stress required to nucleate an hcp martensite from a perfect bcc crystal. The stress levels for hcp nucleation calculated in the present analysis for Ti–6.25at.%Ta and Ti–6.25at.%Nb alloys are 114 MPa and 95 MPa respectively.

1. Introduction

Martensitic transformation is an important class of solid to solid transformation observed in metals [1], ceramics [2], and biological systems [3]. In the present paper, we investigate the bcc–hcp martensitic transformation in two important alloys, Ti–6.25at.% Nb and Ti–6.25at.%Ta. The commonly used Ti alloys, for example Ti–6Al–4V, Co–Cr alloys and stainless steels for biomedical implants contain toxic elements such as vanadium and nickel. Ti–Ta and Ti–Nb alloys are excellent biomaterials possessing high biocompatibility in addition to high corrosion resistance, high strength, and low elastic modulus. [4,5]. Depending on the alloy composition, Ti-alloys exhibit martensitic transformation from a disordered body centered cubic (β) to hexagonal (α') or orthorhombic (α'') crystal structures [6–8]. Experimentally, it is observed that Ta (Nb) concentration below critical 6.9 (7.2) at.% results in the β to α' transformation while Ta/Nb concentration above these compositions results in the β to α'' transformation. To date, no studies have been reported on the bcc–hcp transformation paths in these alloys, and the methodology to determine the hcp nucleation stress is still unresolved. In the present work, we establish the complete energetics of the bcc–hcp nucleation in Ti–6.25at.%Ta and Ti–6.25at.% Nb using first principles energy calculations (Density Functional Theory, DFT). We establish a methodology to obtain the hcp nucleation stress from the parent bcc crystal employing dislocation based martensitic transformation mechanism. We obtain the energy barriers associated with the nucleation process at an atomic scale and combine it with the Peierls Nabarro (PN) formalism to develop a theoretical model. The advantage of such a model is that it is free from any empirical constants.

The bcc–hcp transformation in bcc metals and alloys is described by the well-established Burgers mechanism [9]. The Burgers lattice correspondence of the bcc and hcp phases can be written as follows:

$$(1\,1\,0)_{bcc} \| (0\,0\,0\,1)_{hcp} \quad \text{and} \quad [\bar{1}\,1\,1]_{bcc} \| [\bar{2}\,1\,1\,0]_{hcp}$$

Accordingly, the hcp lattice can be formed from the bcc lattice via two transformation modes as shown in Fig. 1 [10]-(i) Alternate collinear shuffle displacements of every second $(1\,1\,0)_{bcc}$ planes in the $[\bar{1}\,1\,0]_{bcc}$ bcc direction by an amount 2δ (or equivalently alternate and opposite displacements of consecutive $(1\,1\,0)_{bcc}$ planes by an amount δ) and (ii) compression (dilation) of the $(1\,1\,0)_{bcc}$ planes in $\langle 0\,0\,1\rangle$ ($\langle 1\,1\,0\rangle$) directions. The transformation mode (i) produces the ACAC hcp type stacking sequence. Similarly, the transformation mode (ii) can be described by the change in angle (θ) between the two body diagonals of $(1\,1\,0)_{bcc}$ plane with the application of deformation strains η_1 and η_2. The body diagonals on the $(1\,1\,0)_{bcc}$ plane are shown as broken lines in Fig. 1(b to d).

* Corresponding author.
E-mail address: huseyin@illinois.edu (H. Sehitoglu).

http://dx.doi.org/10.1016/j.commatsci.2015.08.050
0927-0256/

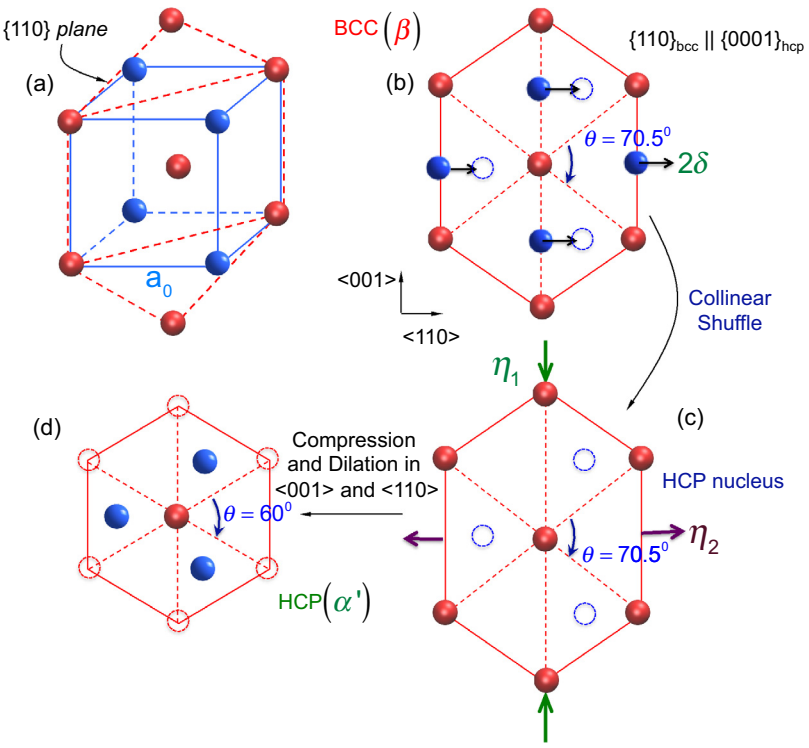

Fig. 1. (a) A bcc unit cell showing the {1 1 0} plane (b) collinear shuffle displacements of {1 1 0} plane in ⟨1 1 0⟩ direction forming an hcp nucleus (c) the hcp nucleus subjected to compression (dilation) in $\langle 001\rangle_{bcc}$ ($\langle 110\rangle_{bcc}$) directions to form (d) an hcp structure.

The complete transformation pathway from bcc–hcp structure can be obtained by simultaneously varying the $\delta - \theta$ parameters. We note that $\delta = 0$ and $\theta = 70.53^{\circ}$ correspond to the bcc structure, while $\delta = \sqrt{2}a_{bcc}/12$ and $\theta = 60^{\circ}$ correspond to the fully formed hcp structure.

2. Methodology

We utilized the Density Functional Theory (DFT) calculations to investigate the energy barriers for the bcc–hcp nucleus transformation. The simulation box consisted of 64 atoms with Ti to Ta/Nb ratio of 15:1. The first-principles total-energy calculations were carried out using the Vienna ab initio Simulations Package (VASP) with the projector augmented wave (PAW) method and the generalized gradient approximation (GGA) [11,12]. PAW is an efficient all electron method which achieves high accuracy when transition elements such as Ti are considered. For lattice constants calculations, a 64 atom supercell with size $4 \times 2 \times 4$ is used. In our simulation, Monkhorst–Pack $5 \times 10 \times 5$ k-point meshes are used for the Brillouin-zone integration. Ionic relaxation was performed by a conjugate gradient algorithm and stopped when absolute values of internal forces were smaller than 5×10^{-3} eV/Å. The energy cut-off of 300 eV was used for the plane-wave basis set. The total energy was converged to less than 10^{-5} eV/atom. In order to generate an alloy model for Ti–6.25at%Ta and Ti–6.25at.%Nb, a simulator code was written to create 64 atoms consisting of two atom types ($n_{Ti} = 60$, $n_{Ta/Nb} = 4$, where n is the number of atoms). It is important to note that the simulation box with 64 atoms is large enough to obtain the converged minimum structural energy value. This was verified with independent simulations with number of atoms ranging from 16 to 96. The atom types were assigned randomly in the periodic supercell, but following the bcc crystal coordinates so that the two atomic positions do not overlap. For lattice constant calculation, the box edges were oriented along the $x = [100]$, $y = [010]$ and $z = [001]$ directions. The effect of random positions of Ta/Nb atoms on lattice constant and minimum structural energies was studied for three independent cases representing three different random solid solution alloys. The results on the structural energies and the lattice constant for these cases were within 2% agreement. The lattice constants and structural energies in Fig. 2 for both Ti–6.25at.%Ta and Ti–6.25at.%Nb are the average of these independent results. The lattice constant of Ti–6.25at.%Ta is 3.246 Å and that of Ti–6.25at.%Nb is 3.239 Å from our calculations, which are within 1% of the experimental values. The experimentally measured lattice constants for both Ti–6.25at.% Ta and Ti–6.25at.% Nb are approximately 3.275 Å [13].

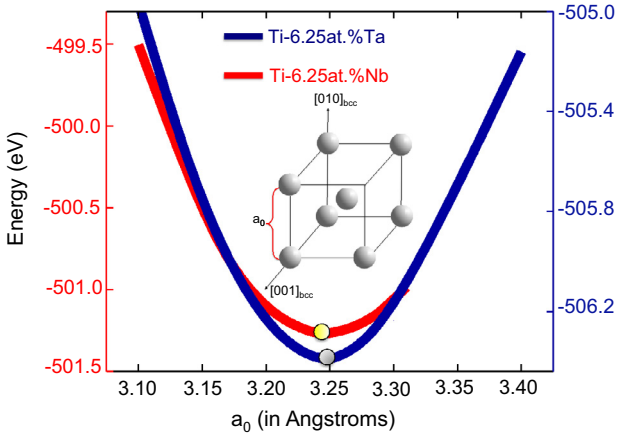

Fig. 2. Energy minimization with respect to lattice parameters variation in Ti–6.25at.%Ta and Ti–6.25at.%Nb alloys.

3. Modeling

As shown previously in Fig. 1, the complete bcc–hcp transformation pathway consists of pure collinear shuffle displacements of the alternate {1 1 0} planes in ⟨1 1 0⟩ directions followed by the compression (and/or dilation) of the {1 1 0} planes. However, as will be discussed later, the repeated shuffle sequence of group of atoms on every second {1 1 0} bcc plane by the same shuffling magnitude (δ) forms the hcp nucleus, and is accounted for while calculating the transformation stress in the present analysis. As shown in Fig. 3(a), the pure shuffling of the atoms is an early stage for dislocation based hcp nucleation, as validated by MD simulations in other bcc metals and alloys [14–16]. In Table 1, we report the corresponding structural energies of the bcc and hcp phases for Ti alloys considered in the present analysis.

We describe the parameter δ representing the collinear shuffle displacements of the bcc atoms on alternate {1 1 0} planes during hcp nucleation based on the heterogeneous dislocation nucleation mechanism. Consider Fig. 3(b) where a pre-existing a/2[1 1 1] dislocation in a bcc crystal dissociates as follows:

$$\frac{a}{2}[1\bar{1}1] \rightarrow \frac{a}{8}[0\bar{1}1] + \frac{a}{8}[0\bar{1}1] + \frac{a}{4}[2\bar{1}1] \quad (1)$$

In fact, the critical stage of martensite nucleation is when the partial dislocations with Burgers vector $b = \frac{a}{8}[0\bar{1}1]$ moves on alternate {1 1 0} bcc plane by an amount δ, leading to the hcp lattice sequence. We undertake first principles energy calculations to establish the energy per unit area required to shuffle the atoms on alternate {1 1 0} planes in terms of a fault energy (γ) curve. It should be noted that the γ -curve we obtain in the present case is associated with the collinear shuffling of the atoms, and is different from the generalized stacking/planar fault energy (GSFE/GPFE) surfaces obtained for slip and twinning in bcc and fcc metals [17–20]. The mechanism where an $a/2\langle 1\,1\,1\rangle$ dislocation split into the partial ones in the {1 1 0} bcc plane and translate to form an hcp nucleus is depicted in Fig. 3(b). The methodology to obtain the nucleation stress based on this heterogeneous mechanism is discussed next.

Table 1
Structural energy difference of bcc and hcp structures for Ti–6.25at.%Ta and Ti–6.25at.%Nb.

Materials	Transformation	E_{bcc} (eV/atom)	E_{hcp} (eV/atom)	$E_{bcc}-E_{hcp}$ (eV/atom)
Ti–6.25at.%Ta	bcc → hcp	−7.924	−7.868	−0.056
Ti–6.25at.%Nb	bcc → hcp	−7.811	−7.729	−0.082

At the nucleation stage, the applied external stress aids the motion of $a/8\ \langle 1\,1\,0\rangle$ dislocations. We are interested in obtaining the critical stress required for hcp nucleation using the modified Peierls Nabarro formalism [21,22]. Consider the single $\frac{a}{2}[1\bar{1}1]$ dislocation in Fig. 3(b) which splits into $\frac{a}{8}[0\bar{1}1]$ dislocations as represented by Eq. (1). We write the total energy of the dislocations as the sum of (i) the elastic energy due to interaction of the dislocations, E_{int} (ii) the self energy of the dislocations, E_{self} (iii) the misfit energy (E^s_γ) which represents the periodic energy that should be overcome by the dislocation, and (iv) the applied work, W, to move the dislocations. Therefore, the total energy of the dislocation configuration in Fig. 3 can be written as follows:

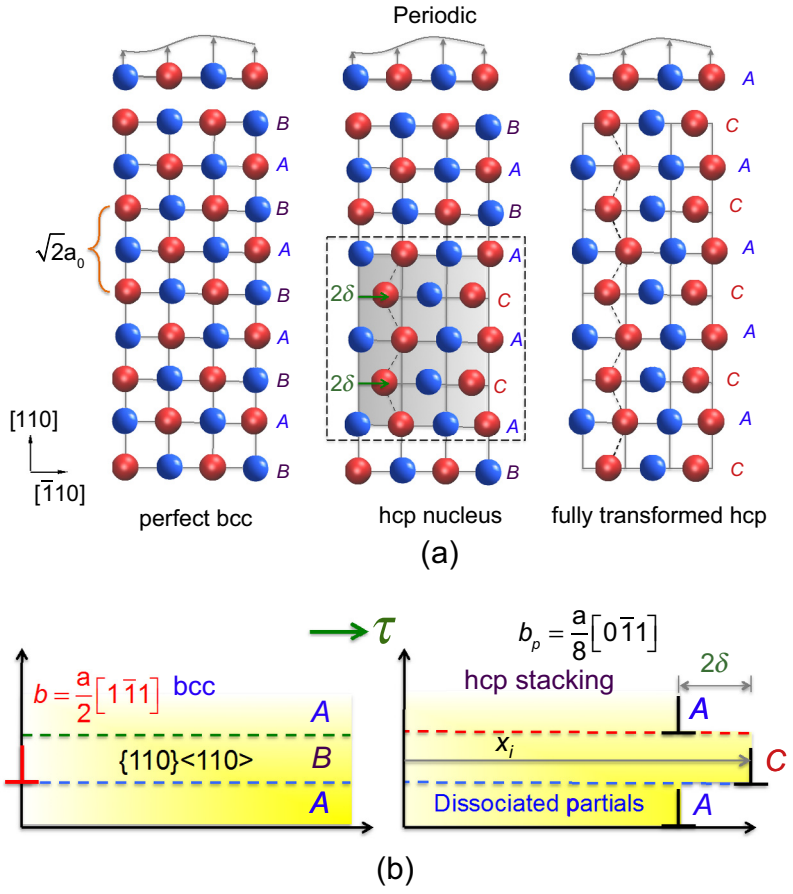

Fig. 3. (A) The formation of an hcp stacking sequence from a perfect bcc crystal. Note that the hcp nucleus is shown by shaded area (b) corresponding dislocation based mechanism where an $\frac{a}{2}[1\bar{1}1]$ dislocation in a bcc crystal dissociates into $\frac{a}{8}[0\bar{1}1]$ partial dislocations forming an hcp nucleus.

$$E_{total} = E_{int} + E_{self} + E^s_\gamma - W$$
$$= -\frac{Gb^2}{2\pi}\ln\left(\frac{2\delta}{r_o}\right) + N\frac{Gb^2}{2(1-\upsilon)}(1-\upsilon\cos^2\theta)$$
$$+ \int_{-\infty}^{+\infty}\gamma[f(x)]dx - 2N\tau b\delta \quad (2)$$

where $E_{self} + E_{int}$ ($=E_{elastic}$) is the elastic strain energy stored in the two half crystals, E^s_γ is the misfit energy representing the periodic non-linear interatomic interactions in the dislocation core [18,23,24], G is the $\{1\,1\,0\}\langle 1\,1\,0\rangle$ shear modulus, and N is the number of dislocations participating in the transformation process. The term E^s_γ is periodic and depends on the position of the dislocation line within the lattice, and the parameter γ is the fault energy landscape associated with the shuffle. By considering the lattice discreteness, the misfit energy E^s_γ can be defined as the sum of all the misfit energies between the pairs of atomic rows as a function of u [25,26]:

$$E^s_\gamma = \sum_{m=-\infty}^{m=+\infty}\gamma(f(ma'-u))a' \quad (3)$$

where a' is the periodicity of E^s_γ and is defined as the shortest distance between two equivalent atomic rows in the direction of the dislocation displacement. The solution to the disregistry function $f(x)$ in the dislocation core is [19,23,27]:

$$f(x) = \frac{b}{\pi}\left\{\tan^{-1}\left(\frac{x}{\zeta}\right) + \tan^{-1}\left(\frac{x-2\delta}{\zeta}\right)\right\} + \frac{b}{2} \quad (4)$$

where $\zeta = h/[2(1-\upsilon)]$ [24] is the half-core width of the dislocation for an isotropic solid, h is the $\{1\,1\,0\}$ interplanar distance and υ is the Poisson's ratio.

We obtained the fault energy curve (γ – curve) for Ti–6.25at.% Ta and Ti–6.25at.%Nb, as shown in Fig. 4(a and b). For γ – curve calculation, a $2\times6\times2$ supercell consisting of 96 atoms is used. The crystal axes are oriented along the $x=[\bar{1}\,1\,0]$, $y=[1\,1\,0]$ and $z=[0\,0\,\bar{1}]$ directions. The supercell consists of 13 $\{1\,1\,0\}$ layers so that the periodic interfaces do not interact. The was verified by conducting sensitivity tests of number of layers (10–13 layers) on stacking fault energies for which no change in stacking fault energy was observed beyond 10 layered supercell. The Monkhorst k-point resolution used is $12\times4\times12$. Four energy terms- $\gamma^u_{sd1}, \gamma^s_{sd1}, \gamma^u_{sd2}$ and γ^s_{sd2} are indicated in Fig. 4(a and b), and the corresponding crystal structures are also shown. The term γ^u_{sd1} in Fig. 4 (a) is the unstable fault energy required to shuffle the Nth layer of the crystal by a displacement of δ. If E_s is the energy of the shuffled lattice corresponding to a normalized shuffle displacement of $\delta/|b|$, and E_o that of the perfect lattice, the fault energy corresponding to any displacement can be calculated from DFT as follows [14]:

$$\gamma = \frac{E_s - E_o}{A_{\{1\,1\,0\}}}$$

where $A_{\{1\,1\,0\}}$ is the area of the $\{1\,1\,0\}$ plane (or y-plane) of the simulation box.

Similarly, γ^s_{sd1} is the stable fault energy per unit area corresponding to the shuffling of the same Nth layer by an additional displacement of δ. It is now important to note that the Nth layer is displaced by a total amount of 2δ. Next, in Fig. 4(b), the already shuffled crystal (on N_{th} layer) is shown to be shuffled further on the $(N+2)_{th}$ layer. The energy term γ^u_{sd2} represents the unstable energy required to shuffle the $(N+2)_{th}$ layer by a displacement of δ. The same $(N+2)_{th}$ layer is shuffled further with a displacement of δ such that the total displacement of the $(N+2)_{th}$ layer is 2δ. The corresponding energy is γ^s_{sd2} which represents the stable fault energy. The energy values associated with the γ -curve corresponding to the shuffling of two layers are given in Table 2. In the present analysis, we undertake the vertical relaxation, which involves the relaxation of atoms perpendicular to the shuffling plane. The vertical relaxation method is employed in the present case compared to full relaxation because the applied shuffling magnitude is small, and during full relaxation, the atoms close to the fault tend to move back to their original positions creating no hcp stacking sequence. In addition, the effect of random positions of solute atoms were also considered for four independent cases. The results showed no significant change in fault energy (within 5%) regardless of the positions of the solutes. The unstable fault energy (γ^u_{sd2}) for Ti–6.25at.%Ta is 280 mJ m^{-2} which is lower than Ti–6.25at.%Nb by 14 mJ m^{-2}. With the γ profile known in the present case, we can subsequently find the misfit energy variation with the dislocation position using Eq. (3), and hence solve for the Peierls stress.

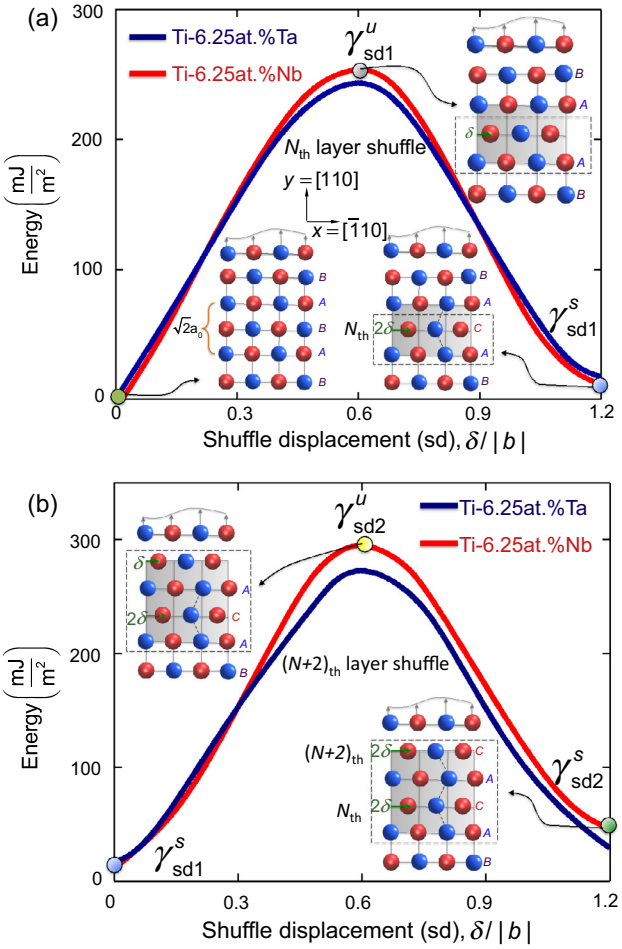

Fig. 4. The γ -curve associated with the normalized collinear shuffle displacement (sd) of (a) Nth layer (b) $(N+2)_{th}$ layer atoms on $\{1\,1\,0\}\langle 1\,1\,0\rangle$bcc plane forming an hcp nucleus. Note $N=1,2,3\ldots$ represents first, second, third (and so on) $\{1\,1\,0\}$ stacking layers in y-direction, and $|b|$ represents the Burgers vector magnitude of the dislocation $b=a/8\ \langle 1\,1\,0\rangle$ participating in the transformation process.

Table 2
Energy terms (in mJ m^{-2}) corresponding to the γ – curve for Ti–6.25at.%Ta and Ti–6.25at.%Nb.

Alloys	γ^u_{sd1}	γ^s_{sd1}	γ^u_{sd2}	γ^s_{sd2}
Ti–6.25at.%Ta	252	19	280	25
Ti–6.25at.%Nb	261	13	294	41

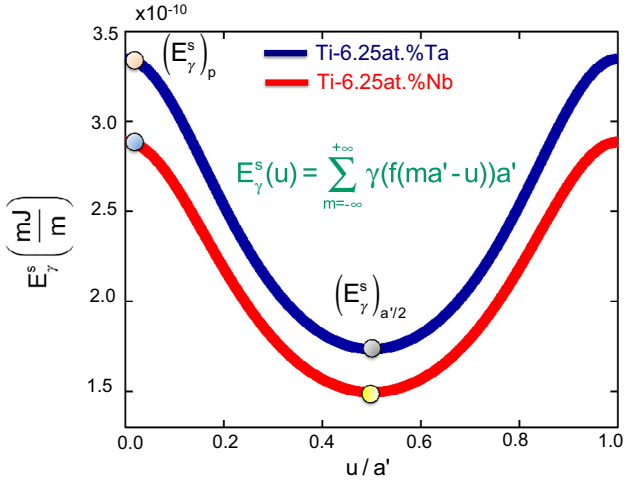

Fig. 5. Misfit energy variation as a function of the dislocation position.

In order to calculate the misfit energy term, E^s_γ, we fit the γ profile using the sine analytical functions. As an example, the fitting function for Ti–6.25at.%Ta in Fig. 4 is:

$$\gamma[f(x)] = \gamma^u_{sd1} \sin\left[0.82\pi \frac{f(x)}{b}\right] \quad \text{for} \quad 0 \leqslant f(x) \leqslant 1.2b \tag{5}$$

$$\gamma[f(x)] = \gamma^u_{sd2} \sin\left[0.79\pi \frac{f(x)}{b} + 0.061\right] \quad \text{for} \quad 0 \leqslant f(x) \leqslant 1.2b \tag{6}$$

Eq. (5) represents the fitting function corresponding to Fig. 4(a) and Eq. (6) represents that of Fig. 4(b). Upon substituting the expressions ((5), (6)) into Eq. (3), we can numerically solve for the misfit energy, and the result is shown in Fig. 5. We also calculated the nucleation stress based on the Peierls theory, which depends only on the misfit energy. Because the elastic strain energy, $E_{elastic}$ is independent of u, the Peierls stress τ_p is then given by the maximum stress required to overcome the periodic barrier in $E^s_\gamma(u)$:

$$\tau_p = \max\left\{\frac{1}{b}\left(\frac{\partial E^s_\gamma}{\partial u}\right)\right\} \tag{7}$$

The stresses calculated based on the Peierls theory for Ti–6.25at.%Ta and Ti–6.25at.%Nb are 348 and 297 MPa respectively. Similarly, upon minimizing Eq. (2) with respect to δ, we numerically evaluate the critical hcp nucleation stress levels, and are presented in Table 3. In the present study, the critical hcp nucleation stress is determined as follows:

$$\frac{\partial E_{total}}{\partial \delta} = 0 \tag{8}$$

The parameters $(E^s_\gamma)_p$ and $(E^s_\gamma)_{a'/2}$ shown in Fig. 5 are also reported in Table 3. The term $(E^s_\gamma)_{a'/2}$ is the minimum of the E^s_γ function and provides an estimate of the core energy of the dislocation. The term $(E^s_\gamma)_p$ is the Peierls energy which is the amplitude of the variation of the energy barrier required to move the dislocation [24]. It is seen from the present calculations (Table 3) that both the terms $(E^s_\gamma)_p$ and $(E^s_\gamma)_{a'/2}$ are lower for the case of Ti–6.25at.%Nb compared to Ti–6.25at.%Ta.

4. Results and discussion

In the present case, the hcp nucleation stress obtained by minimizing Eq. (2) for Ti–6.25at.%Ta is 114 MPa while that for Ti–6.25at.%Nb is 95 MPa. It is interesting to note that the nucleation stress magnitudes of Ti–6.25at.%Ta and Ti–6.25at.%Nb differ only by 19 MPa, and is much lower than the stress levels predicted by the Peierls theory. Experimentally, the flow stress magnitude in the case of Ti–Ta alloy is observed to be 350–360 MPa [28]. However, this value does not correspond to the critical resolved shear stress for hcp nucleation. Nonetheless, if we consider that the Schmid factor on $\{1\,1\,0\}\langle 1\,1\,0\rangle$ bcc system is maximum, i.e. 0.5, we obtain the nucleation stress of 175 MPa experimentally compared to the theoretical value of 114 MPa. Another source of difference is that the experiments report 0.2% offset value and smaller offsets would lower the 175 MPa value. Interestingly, additional experiments have shown that the flow stress for bcc-orthorhombic (α'') transformation in the case of Ti–22at.%Nb is approximately 300–400 MPa [29]. It is worth pointing out that the theoretical stress value for the bcc–hcp transformation in the case of Ti–6.25at.%Nb is comparable to the one for bcc- α'' transformation.

We note that the stresses reported in Table 3 are based on the modified Peierls Nabarro formalism of dislocation motion. In the present calculation, the assumption that the hcp nucleus is formed by the motion of split $a/2\ \langle 1\,1\,1\rangle$ dislocation is based on the heterogeneous martensite nucleation theory supported by molecular dynamics simulations [14–16]. Such observations have highlighted the role of dislocations in bcc–hcp transformation. The atomistic simulation of the bcc–hcp transformation in Zr [15] has been carried out in the presence of two types of dislocations, $\langle 1\,0\,0\rangle$ and $\langle 1\,1\,1\rangle$, and in the absence of dislocations, no bcc–hcp transformation occurred even after a long period of simulation time. The total dynamics of such observations can be considered as a nucleation event where the hcp stacking sequence is first formed from pre-existing dislocations following the compression/dilation of the basal plane requiring no dislocation activities.

It is should be noted that the present analysis is based on the notion that the presence of the lattice defects such as free surfaces, dislocations, inclusions promotes the martensitic transformation [30,31]. Note that the dislocations considered in the present analysis are straight, and only have edge component. The faulting due to the presence of dislocations makes the initial bcc phase much closer to the hcp structure of a martensite, thus reducing the transformation barrier as observed in other Ti-alloys [16].

5. Conclusion

To conclude, we established the energy barrier of the bcc–hcp martensitic nucleation in Ti–6.25at.% and Ti–6.25at.%Nb using first principles energy calculations in the form of a γ -curve.

Table 3
Critical bcc–hcp nucleation stress for Ti–6.25at.%Ta and Ti–6.25at.%Nb.

Materials	Burgers vector (Å)	$(E^s_\gamma)_p \times 10^{-10}$ mJ m^{-1}	$(E^s_\gamma)_{a'/2} \times 10^{-10}$ mJ m^{-1}	Critical nucleation stress (MPa)	
				Peierls Theory, τ_p	Present study, τ_{crit}
Ti–6.25at.%Ta	0.574	3.41	1.78	348	114
Ti–6.25at.%Nb	0.573	2.90	1.55	297	95

We obtained theoretically the hcp nucleation stress from a perfect bcc crystal using modified Peierls Nabarro formalism and the heterogeneous nucleation mechanism. The methodology can be applied to a variety of other bcc metals and alloys. The theoretical model developed in this analysis is free of any empirical constants.

Acknowledgements

This work was partially supported by the National Science Foundation, NSF CMMI-1300284 and the Nyquist Chair funds from the Department of Mechanical Science and Engineering.

References

[1] K. Otsuka, C.M. Wayman, Shape Memory Materials, Cambridge University Press, 1999.
[2] P.M. Kelly, L.R.F. Rose, Progr. Mater. Sci. 47 (2002) 463–557.
[3] G.B. Olson, H. Hartman, Le Journal de Physique Colloques 43 (1982). C4-855-C854-865.
[4] T. Ozaki, H. Matsumoto, S. Watanabe, S. Hanada, Mater. Trans. 45 (2004) 2776–2779.
[5] Y.L. Hao, S.J. Li, S.Y. Sun, C.Y. Zheng, Q.M. Hu, R. Yang, Appl. Phys. Lett. 87 (2005) 091906.
[6] T. Ahmed, H.J. Rack, J. Mater. Sci. 31 (1996) 4267–4276.
[7] K.A. Bywater, J.W. Christian, Philos. Mag. 25 (1972) 1249–1273.
[8] W. Xu, K.B. Kim, J. Das, M. Calin, B. Rellinghaus, J. Eckert, Appl. Phys. Lett. 89 (2006) 031906.
[9] W.G. Burgers, Physica 1 (1934) 561–586.
[10] M. Ekman, B. Sadigh, K. Einarsdotter, P. Blaha, Phys. Rev. B 58 (1998) 5296.
[11] G. Kresse, J. Furthmüller, Phys. Rev. B 54 (1996) 11169–11186.
[12] G. Kresse, J. Hafner, Phys. Rev. B 48 (1993) 13115–13118.
[13] A.V. Dobromyslov, V.A. Elkin, Scr. Mater. 44 (2001) 905–910.
[14] Y.N. Gornostyrev, M.I. Katsnel'son, A.R. Kuznetsov, A.V. Trefilov, J. Exp. Theor. Phys. Lett. 70 (1999) 380–384.
[15] A.R. Kuznetsov, Y.N. Gornostyrev, M.I. Katsnelson, A.V. Trefilov, Mater. Sci. Eng.: A 309 (2001) 168–172.
[16] M. Grujicic, P. Dang, Mater. Sci. Eng.: A 205 (1996) 153–165.
[17] V. Vitek, Philos. Mag. 18 (1968) 773–786.
[18] S. Ogata, J. Li, S. Yip, Phys. Rev. B 71 (2005) 224102.
[19] A. Ojha, H. Sehitoglu, Philos. Mag. Lett. 94 (2014) 647–657.
[20] A. Ojha, H. Sehitoglu, L. Patriarca, H.J. Maier, Modell. Simul. Mater. Sci. Eng. 22 (2014) 075010.
[21] G. Lu, N. Kioussis, V.V. Bulatov, E. Kaxiras, Philos. Mag. Lett. 80 (2000) 675–682.
[22] R. Peierls, Proc. Phys. Soc. 52 (1940) 34.
[23] G. Schoeck, physica status solidi (b) 248 (2011) 2284–2289.
[24] B. Joós, Q. Ren, M.S. Duesbery, Phys. Rev. B 50 (1994) 5890–5898.
[25] Y.-M. Juan, E. Kaxiras, Philos. Mag. A 74 (1996) 1367–1384.
[26] E.B. Tadmor, R.E. Miller, Modeling Materials: Continuum, Atomistic and Multiscale Techniques, Cambridge University Press, 2011.
[27] B. Joos, M.S. Duesbery, Phys. Rev. Lett. 78 (1997) 266.
[28] Y.L. Zhou, M. Niinomi, T. Akahori, Mater. Sci. Eng.: A 371 (2004) 283–290.
[29] S. Miyazaki, H.Y. Kim, H. Hosoda, Mater. Sci. Eng.: A 438 (2006) 18–24.
[30] G.B. Olson, M. Cohen, Metall. Trans. A 7 (1976) 1905–1914.
[31] G.B. Olson, M. Cohen, Metall. Trans. A 7 (1976) 1897–1904.